

SCIENTIFIC REPORTS



OPEN

Contrast-enhanced transrectal ultrasound for prediction of prostate cancer aggressiveness: The role of normal peripheral zone time-intensity curves

Received: 22 June 2016
Accepted: 11 November 2016
Published: 08 December 2016

Hui Huang^{1,*}, Zheng-Qiu Zhu^{1,*}, Zheng-Guo Zhou¹, Ling-Shan Chen², Ming Zhao³, Yang Zhang⁴, Hong-Bo Li¹ & Li-Ping Yin^{1,4}

To assess the role of time-intensity curves (TICs) of the normal peripheral zone (PZ) in the identification of biopsy-proven prostate nodules using contrast-enhanced transrectal ultrasound (CETRUS). This study included 132 patients with 134 prostate PZ nodules. Arrival time (AT), peak intensity (PI), mean transit time (MTT), area under the curve (AUC), time from peak to one half (TPH), wash in slope (WIS) and time to peak (TTP) were analyzed using multivariate linear logistic regression and receiver operating characteristic (ROC) curves to assess whether combining nodule TICs with normal PZ TICs improved the prediction of prostate cancer (PCa) aggressiveness. The PI, AUC ($p < 0.001$ for both), MTT and TPH ($p = 0.011$ and 0.040 respectively) values of the malignant nodules were significantly higher than those of the benign nodules. Incorporating the PI and AUC values (both, $p < 0.001$) of the normal PZ TIC, but not the MTT and TPH values ($p = 0.076$ and 0.159 respectively), significantly improved the AUC for prediction of malignancy (PI: 0.784–0.923; AUC: 0.758–0.891) and assessment of cancer aggressiveness ($p < 0.001$). Thus, all these findings indicate that incorporating normal PZ TICs with nodule TICs in CETRUS readings can improve the diagnostic accuracy for PCa and cancer aggressiveness assessment.

Prostate cancer (PCa) is the second most common malignant tumour that affects the male population¹. Timely diagnosis of PCa can ensure efficient management of the disease and improve active surveillance in patients with and without clinically significant cancers². Consequently, the precise evaluation of prostate nodules is vital.

Contrast-enhanced transrectal ultrasound (CETRUS) has been used widely to enhance the visualization of perfusion changes related to PCa, and it is regarded as a promising tool for evaluating malignant prostate nodules³. In clinical practice, PCa is confirmed or excluded by transrectal ultrasound-targeted biopsy, based on the results of digital rectal examination or serum prostate-specific antigen (PSA) levels⁴, and perfusion analysis by CETRUS⁵. However, recent findings have demonstrated that CETRUS is of limited value for evaluating the aggressiveness of PCa, owing to its varying sensitivity and specificity^{5,6}.

PCa generally exhibits altered angiogenic microvascular structures and blood flow patterns, which characterize the aggressiveness of this cancer and form the basis of diagnosis based on CETRUS^{7,8}. However, the flow pattern signals of this malignancy are often subtle and disappear within seconds; the efficiency of this method is therefore highly user dependent. Therefore, quantitative techniques that extract perfusion parameters to distinguish between malignant and benign tissue are being developed from CETRUS recordings: one of these techniques is the creation of time-intensity curves (TICs). TICs include many crucial parameters, such as arrival time (AT)⁹, mean transit time (MTT) and rise time¹⁰, time to peak (TTP) and peak intensity (PI)⁹, among others.

¹Department of Ultrasound, Affiliated Hospital of Nanjing University of TCM, Nanjing 210029, China. ²Department of Radiology, Affiliated Hospital of Nanjing University of TCM, Nanjing 210029, China. ³Department of Pathology, Affiliated Hospital of Nanjing University of TCM, Nanjing 210029, China. ⁴Department of Urology, Affiliated Hospital of Nanjing University of TCM, Nanjing 210029, China. *These authors contributed equally to this work. Correspondence and requests for materials should be addressed to L.-P.Y. (email: yinliping003@aliyun.com)

These quantitative indices are reported to have high diagnostic accuracy and lesser user dependency. However, the discriminative power of these indices depends in part on the “background” variability of tissue heterogeneity, which when eliminated improves the diagnostic accuracy of magnetic resonance imaging (MRI) for PCa detection¹¹. However, to date, although CETRUS is a commonly used modality for the diagnosis of malignant prostate nodules, TICs of the normal peripheral zone (PZ) are still rarely taken into account.

Therefore, the aim of this study was to evaluate the role of normal PZ TICs for the detection of PCa and assessment of cancer aggressiveness, and to determine whether the diagnostic accuracy improves significantly, compared to the biopsy findings, when normal PZ quantitative parameters are incorporated.

Material and Methods

This study was approved by the ethics committee of the Jiangsu Province Hospital of Traditional Chinese Medicine, and the methods were carried out in accordance with the relevant guidelines. Written informed consent was obtained from all patients.

Patients. Between May 2014 and March 2016, 132 patients with abnormal digital rectal examination findings and/or elevated serum PSA levels (≥ 4 ng/ml and ≤ 10 ng/ml) who had not previously undergone biopsy were enrolled in this study. All the patients underwent CETRUS, which was performed by an experienced operator, and all the CETRUS data were independently reviewed frame by frame on the scanner by two other experienced investigators who were blinded to the greyscale imaging and pathological results. Then, a systematic twelve-core transrectal ultrasound-guided prostate biopsy and two-core targeted biopsy were performed based on the abnormal sonography findings by an experienced operator from the Department of Urology, who was assisted by the CETRUS operator mentioned earlier.

CETRUS procedure. Each patient was evaluated using ultrasonography at the baseline and again during intravenous infusion of sulphur hexafluoride microbubbles (SonoVue; Bracco, Milan, Italy) (Fig. 1a,b). An IU-22 ultrasound system (Philips, Amsterdam, The Netherlands) with a transrectal end-fire transducer (c8-4v) was used. Normal greyscale imaging was performed with a probe frequency of 4 to 8 MHz and a dynamic range of 55 dB. For colour Doppler ultrasonography, the probe frequency was 6 MHz, and the colour Doppler gain was adjusted to maximize signal but eliminate colour noise from the tissue of the prostate. The colour Doppler window was set to include the entire gland. During the contrast-enhanced ultrasound examinations, a fast bolus injection of 2.4 ml SonoVue was administered intravenously; this was followed by administration of 5 ml of normal saline flush. The scanner was set in the contrast pulse-sequencing mode with a probe frequency of 8 MHz. The acoustic power was set at a mechanical index of 0.13, and the dynamic range was fixed at 55 dB. The transverse plane of the sonographic abnormality was chosen for contrast imaging. In patients with no suspicious baseline ultrasonography results, the most hypervascular plane on colour Doppler images was chosen. The entire examination was saved in a Digital Imaging and Communications in Medicine format and transmitted to a workstation for further analysis (Fig. 1c).

Image analysis. All CETRUS data were analyzed on the workstation using the QLAB quantification software (Philips) by a sonographer who was blinded to all the clinical and pathological information (Fig. 1c). Considering that the enhancement characteristics of the PZ lesions were completely different from those of the transition zone lesions, which may reflect the hypervascularity of the normal inner gland and coexisting benign prostate hyperplasia, only the PZ was evaluated in this study. Therefore, duplicated regions of interest (ROIs) were drawn in the targeted biopsy and normal PZ site on contrast ultrasonographic images, and the diameters were set to approximately 5 mm. The TICs were reconstructed for each ROI, and then the relative quantitative parameters, which depicted the features of prostate tissue perfusion in the ROI that were observed after time zero, were measured by three well-trained observers. The average of all the measurements was calculated.

Analysis of oncological outcomes. Biopsy specimens were labelled according to the location from which they were obtained and fixed with a 10% formaldehyde solution in separate test tubes. The pathological findings were assessed by an experienced pathologist as benign prostatic hyperplasia, acute or chronic prostatitis, or prostatic intraepithelial neoplasia or carcinoma (Fig. 1d). The grade of the tumour was also evaluated and assigned a standard Gleason score (Table 1).

Statistical analysis. Student's *t*-test was used to analyze differences in the quantitative parameters of TICs between benign and malignant lesions (Table 2). Multivariate logistic regression was used to test our first hypothesis: joint analysis of the nodule TICs (e.g. PI in this section) and the normal PZ PI results in better prediction of PCa. We can express the regression model for the probability of malignancy as follows:

$$z = C + B_D PI_D \quad (1)$$

$$z = C + B_D PI_D + B_N PI_N \quad (2)$$

$$p = e^z / (1 + e^z) \quad (3)$$

Eqs (1) and (2) are the regression equations calculated for the model using nodule PI only and the nodule and normal PZ PI together. The subscripts *D* and *N* represent the nodule and normal PZ, respectively. *B* and *C* represent the regression coefficient and regression constant, respectively, that correspond to these variables. Subsequently, the *z* values are calculated from Eqs (1) and (2), and the continuous variables are converted

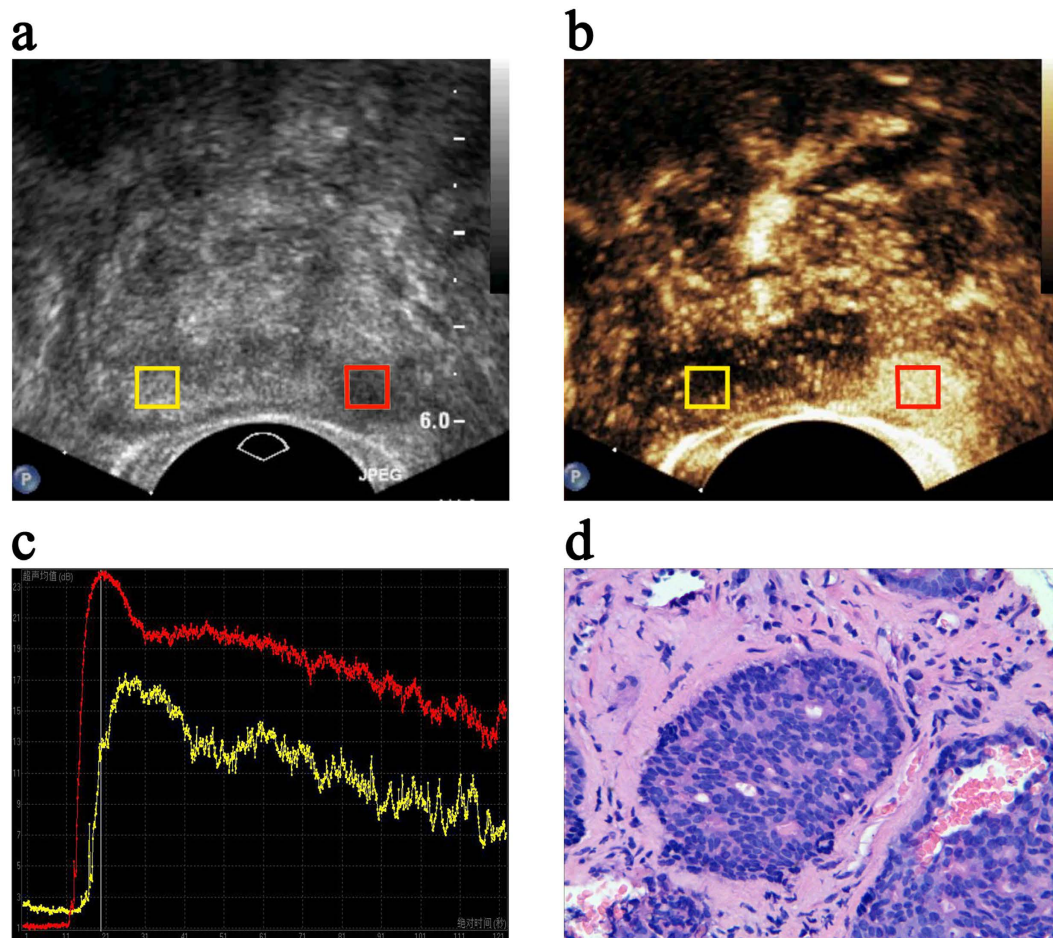


Figure 1. The region of interest (ROI) settings, time-intensity curve (TIC) analysis and oncological outcomes. Transverse (a) greyscale and (b) contrast-enhanced transrectal ultrasound mapping of the prostate in a 67-year-old patient. The red box indicates the ROI placed in the nodule lesion, and the yellow box indicates the corresponding ROI placed in the normal peripheral zone (PZ). (c) The red and yellow lines in the TICs represent the perfusion characteristics of the ROIs of the nodules and the normal PZ, respectively. (d) The oncological outcomes following biopsy show an adenocarcinoma.

Characteristic	Value		
No. of patients	132		
No. of PZ nodules	134		
Clinical characteristics*	Benign lesions** (n = 80)	Malignant lesions (n = 54)	p value
Age (y)	65.9 ± 9.0	67.1 ± 10.8	0.475
PSA (ng/ml)	5.2 ± 3.0	5.9 ± 3.1	0.211
Prostate volume (cm ³)	50.1 ± 26.5	43.3 ± 13.1	0.206
Gleason score	No. of lesions, n (%)		
5	4 (7.4)		
6	19 (35.2)		
7	21 (38.9)		
8	7 (13.0)		
9	3 (5.5)		

Table 1. Clinical and pathologic characteristics of the patients. PZ: peripheral zone, PSA: prostate-specific antigen. *Data are shown as the mean ± standard deviation. **Benign: 76, benign prostatic hyperplasia; 4, chronic prostatitis.

Parameters	Nodules (n = 130)			Normal peripheral zone (n = 130)		
	Benign lesions (n = 76)	Malignant lesions (n = 54)	p value	Benign lesions (n = 76)	Malignant lesions (n = 54)	p value
AT (s)	22.0 ± 6.0	22.7 ± 4.8	0.512	21.7 ± 6.4	21.8 ± 5.7	0.913
PI (dB)	12.6 ± 4.4	17.2 ± 3.9	<0.001	13.4 ± 4.8	11.8 ± 3.6	0.052
MTT (s)	32.3 ± 9.8	37.0 ± 10.4	0.011	30.4 ± 9.5	33.9 ± 9.2	0.036
AUC (dB/s)	685.1 ± 334.1	1055.3 ± 404.4	<0.001	705.5 ± 362.8	699.1 ± 273.3	0.912
TPH (s)	46.5 ± 15.7	52.3 ± 15.8	0.040	44.3 ± 15.0	48.4 ± 14.2	0.119
WIS (dB/s)	1.4 ± 0.6	1.5 ± 0.6	0.612	1.5 ± 0.8	1.1 ± 0.6	0.001
TTP (s)	32.4 ± 8.2	30.5 ± 5.9	0.149	31.7 ± 9.1	33.7 ± 7.3	0.198

Table 2. Quantitative parameters of the nodule and normal peripheral zone time-intensity curves. AT: arrival time; PI: peak intensity; MTT: mean transit time; AUC: area under the curve; TPH: time from peak to one half; WIS: wash in slope; TTP: time to peak. Values are shown as the mean ± standard deviation.

Parameters		B _D		B _N		C	
		Value	p value	Value	p value	Value	p value
AT	AT _D only	0.021	0.509	—	—	−0.816	0.271
	AT _D + AT _N	0.023	0.508	−0.004	0.903	−0.764	0.369
PI	PI _D only	0.275	<0.001	—	—	−4.502	0.007
	PI _D + PI _N	0.716	<0.001	−0.586	<0.001	−3.490	0.001
MTT	MTT _D only	0.046	0.014	—	—	−1.947	0.004
	MTT _D + MTT _N	0.037	0.076	0.023	0.285	−2.374	0.003
AUC	AUC _D only	0.003	<0.001	—	—	−2.715	<0.001
	AUC _D + AUC _N	0.009	<0.001	−0.008	<0.001	−1.985	0.001
TPH	TPH _D only	0.024	0.041	—	—	−1.541	0.013
	TPH _D + TPH _N	0.021	0.159	0.005	0.750	−1.629	0.017
WIS	WIS _D only	0.156	0.253	—	—	−0.566	0.239
	WIS _D + WIS _N	0.479	0.163	−1.043	0.001	0.295	0.595
TTP	TTP _D only	−0.036	0.151	—	—	0.802	0.323
	TTP _D + TTP _N	−0.056	0.050	0.045	0.061	−0.061	0.948

Table 3. Multivariate logistic regression of the quantitative parameters of TICs based on Eqs (1 and 2). AT: arrival time; PI: peak intensity; MTT: mean transit time; AUC: area under the curve; TPH: time from peak to one half; WIS: wash in slope; TTP: time to peak. D = nodule peripheral zone tissue, N = normal peripheral zone tissue, B = regression coefficient, C = regression constant.

from the two categorical dependent variables (benign or malignant) to calculate the probability of malignancy. However, the range of values from positive to negative is large, which makes comparison difficult. Therefore, Eq. (3) represents *Poisson's* conversion from z to the probability of malignancy, p , which ranged from 0 to 1. The PI_D and PI_N values and the significance of these variables in the multivariate logistic regression model are presented in Table 3.

Our second hypothesis was that the improved prediction of PCa results in a significant improvement in diagnostic accuracy in differentiating between benign and malignant nodules. Utilizing the receiver operating characteristic (ROC) curves constructed from malignant probability (p) values, we created a standalone PI_D regression model based on Eq. (1) and a joint regression model incorporating PI_N from Eq. (2) to compare diagnostic accuracy. The differences between areas under the ROC curve were calculated using statistical methods described by DeLong *et al.*¹² and Hanley *et al.*¹³ Furthermore, a visual assessment of the correlation between nodule PI and normal PZ PI was provided by plotting the benign and malignant nodules with respect to their PI and the corresponding normal PZ PI.

Our third hypothesis was that including normal PZ TICs significantly improves the differentiation of cancer aggressiveness between low-grade and high-grade tumours. Generally, tumours with a Gleason score of 7, 8 or 9 are defined as high-grade tumours, whereas tumours with a Gleason score of 5 or 6 are defined as low-grade tumours^{11,14}. Using box plot analysis, we established a standalone PI_D regression model and incorporated the PI_N model into it to compare the probability of malignancy (p) and test for significant differences.

All statistical analyses were carried out using SPSS Statistics, version 18 (IBM, Chicago, USA). $P < 0.05$ was considered to indicate statistical significance.

Results

Clinical and pathological characteristics. The clinical and pathological characteristics of 132 patients with 134 nodules are listed in Table 1. The results of pathologic examination of the target biopsy samples revealed that there were 54 malignant and 80 benign lesions. Of the 80 benign lesions, 4 nodules were excluded from

Parameters		Sensitivity (%)	Specificity (%)	PPV (%)	NPV (%)	AUC (%)
PI	PI _D only	66.7 (36/54)	73.7 (56/76)	64.3 (36/56)	75.7 (56/74)	78.4 (70.4–86.5)
	PI _D + PI _N	79.6 (43/54)	90.8 (69/76)	86.0 (43/50)	86.3 (69/80)	92.3 (87.6–96.9)
AUC	AUC _D only	53.7 (29/54)	81.6 (62/76)	67.4 (29/43)	71.3 (62/87)	75.8 (67.3–84.3)
	AUC _D + AUC _N	72.2 (39/54)	92.1 (70/76)	86.7 (39/45)	82.4 (70/85)	89.1 (83.2–95.1)

Table 4. Diagnostic performance of the nodule parameters only and both the nodule parameters and normal peripheral zone PI or AUC. PI: peak intensity, AUC: area under the curve, PPV: positive predictive value, NPV: negative predictive value. D = nodule peripheral zone tissue, N = normal peripheral zone tissue. The AUC values are followed by the 95% CIs in parentheses.

further analysis as they were identified as chronic prostatitis nodules ($n = 4$). There was no significant difference between the benign and malignant groups with regard to age, PSA and prostate volume ($p = 0.475$, 0.211 and 0.206 , respectively). Among the 54 malignant lesions, four lesions had a Gleason score of 5 (7.4%, 4 of 54); 19 lesions had a Gleason score of 6 (35.2%, 19 of 54); 21 lesions, 7 (38.9%, 21 of 54); seven lesions, 8 (13.0%, 7 of 54); and three lesions, 9 (5.5%, 3 of 54).

Analysis of the quantitative parameters of TICs. The results of analysis of the quantitative parameters of prostate lesions and normal PZ TICs are shown in Table 2. Total TIC analysis showed that PI ($p < 0.001$), MTT ($p = 0.011$), area under the curve (AUC) ($p < 0.001$) and time from peak to one half (TPH) ($p = 0.040$) were significantly higher in the malignant nodules than in the benign nodules, but AT, wash in slope (WIS) and TTP were not significantly higher ($p = 0.512$, 0.612 , and 0.149 , respectively; Table 2). Moreover, the TIC parameters of normal PZ tissue were not significantly different between benign and malignant lesions, except for MTT and WIS ($p = 0.036$ and 0.001 , respectively; Table 2). Multivariate logistic regression analysis showed that nodule PI ($p < 0.001$), MTT ($p = 0.014$), AUC ($p < 0.001$) and TPH ($p = 0.041$) were significant factors with regard to the prediction of PCa, but AT, WIS and TTP were not significant factors ($p = 0.509$, 0.253 and 0.151 , respectively; Table 3).

The effect of incorporating normal PZ PI, AUC, MTT or TPH in the prediction of PCa. Normal PZ TICs, which reflect the “background” characteristics of prostate tissue, are correlated with the TICs of PZ in prostate nodules. By using logistic regression and Eqs (1) and (2), a regression model using only nodule TIC parameters can be expressed as Eqs (4) and (5), shown below:

$$z = -4.502 + 0.275PI_D \quad (4)$$

$$z = -2.715 + 0.003AUC_D \quad (5)$$

The model incorporating PI_D and PI_N or AUC_D and AUC_N can be expressed as Eqs (6) and (7) respectively:

$$z = -3.490 + 0.716PI_D - 0.586PI_N \quad (6)$$

$$z = -1.985 + 0.009AUC_D - 0.008AUC_N \quad (7)$$

In both regression models, a dramatic change was introduced by the addition of nodule PI ($p < 0.001$, PI_D alone; $p < 0.001$, PI_D including PI_N, Table 3), nodule AUC ($p < 0.001$, AUC_D alone; $p < 0.001$, AUC_D including AUC_N, Table 3), normal PZ PI ($p < 0.001$; Table 3) and AUC ($p < 0.001$; Table 3); this significantly improved the prediction of malignancy. Table 4 and Fig. 2a show the ROC curves for the probability value p based on the regression models of Eqs (4) and (6): the area under the ROC curve increased by 17.7%, from 0.784 (95% CI, 0.704–0.865) to 0.923 (95% CI, 0.876–0.969) ($p < 0.001$, according to both the DeLong and Hanley methods). Table 4 and Fig. 2b show that the area under the ROC curve based on the regression models of Eqs (5) and (7) increased by 17.5%, from 0.758 (95% CI, 0.673–0.843) to 0.891 (95% CI, 0.832–0.951) ($p < 0.001$, according to both the DeLong and Hanley methods).

However, incorporating the normal MTT or TPH ($p = 0.285$, MTT_N; $p = 0.750$, TPH_N; Table 3) failed to improve the prediction accuracy of PCa.

Diagnostic accuracy of the regression models. Incorporating PI_N dramatically improved tumour diagnostic accuracy ($p < 0.001$; PI_D only, $p < 0.001$), as did the inclusion of AUC_N ($p < 0.001$; AUC_D only, $p < 0.001$). When only PI_D was incorporated into the regression model, the specificity, sensitivity, positive predictive value (PPV) and negative predictive value (NPV) were 73.7%, 66.7%, 64.3% and 75.7%, respectively; when PI_N was also included, these values increased to 90.8% (69 of 76), 79.6% (43 of 54), 86.0% (43 of 50) and 86.3% (69 of 80), respectively. Similarly, when only AUC_D was incorporated in the regression model, the specificity, sensitivity, PPV and NPV were 81.6%, 53.7%, 67.4% and 71.3%, respectively; when AUC_N was also incorporated, these values increased to 92.1% (70 of 76), 72.2% (39 of 54), 86.7% (39 of 45), and 82.4% (70 of 85), respectively.

Correlation between nodule TICs and normal PZ TICs. In combination with Eq. (3), the regression models established depict the probability of a given nodule being a prostatic malignancy. Based on the models

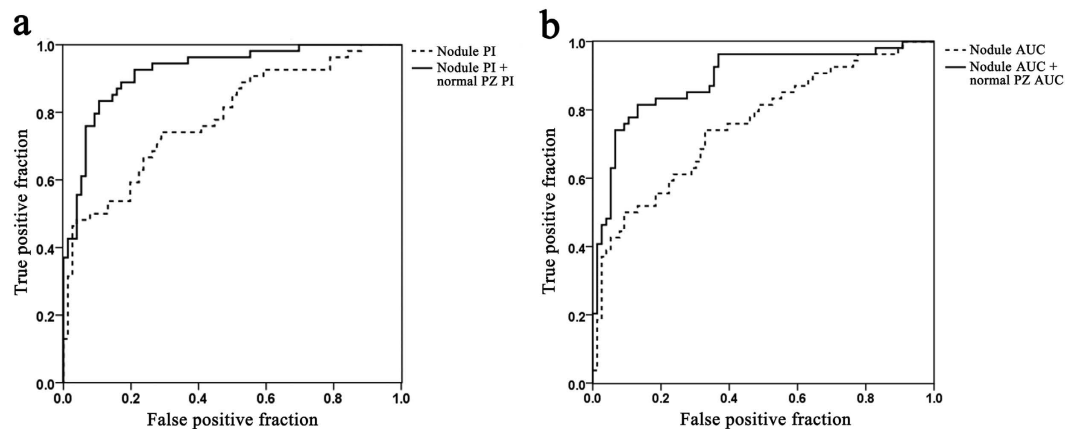


Figure 2. Receiver operating characteristic curve of the regression models based on Eq. (3). The solid line shows the diagnostic accuracy when the model incorporates (a) the normal peripheral zone (PZ) peak intensity (PI) in addition to the nodule PIs and (b) the normal PZ area under the curve (AUC) in addition to the nodule AUCs. The dotted line shows the diagnostic accuracy of (a) nodule PIs only and (b) nodule AUCs only.

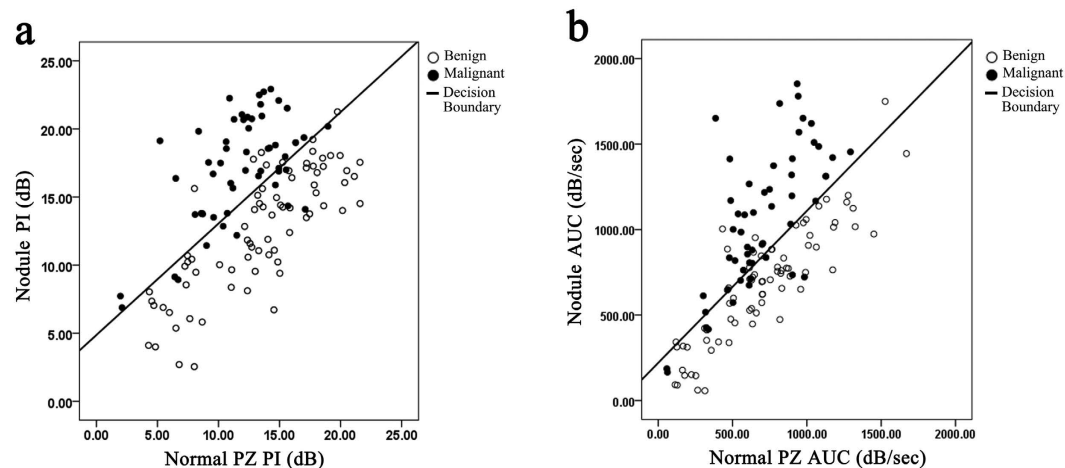


Figure 3. Scatter plots and decision boundary of the (a) model incorporating the nodule peak intensity (PI) and the normal peripheral zone (PZ) PI and (b) the model incorporating the nodule area under the curve (AUC) and the normal PZ AUC. The line represents the decision boundary; the solid dots, the malignant lesions; and the looped dots, the benign lesions.

that also incorporate PI_N or AUC_N (Fig. 3a,b), it seems that a relatively low PI_D or AUC_D might still be indicative of a highly suspicious tumour if the PI_N or AUC_N is also low. Thus, the diagnostic accuracy of a threshold based on only the PI_D or AUC_D value alone may not be very high (decision line in Fig. 3a,b).

Assessment of cancer aggressiveness based on the regression models. Based on the probability of malignancy (p) of the regression models, it seems that both the PI_D only and PI_D plus PI_N models are significant with regard to differentiating between low-grade tumours and benign lesions ($p < 0.001$ for both, Fig. 4a,b). Moreover, the PI_D plus PI_N model is significant for differentiating between high-grade tumours and benign lesions ($p < 0.001$, Fig. 4b), but the PI_D only model is not ($p = 0.080$, Fig. 4a). Moreover, the inclusion of nodule PI along with normal PZ PI resulted in a significant improvement in the differentiation of high-grade tumours from benign nodules ($p < 0.001$ for both, Fig. 4a,b).

Discussion

Several studies have reported that CETRUS has high diagnostic sensitivity and specificity for the prediction of PCa^{9,10}. However, with regard to TICs, the most accurate quantitative parameters differ greatly from each other^{9,10}, which means that the diagnostic accuracy of the parameters vary. In this study, we found that the perfusion indices PI, MTT, AUC and TPH are significant factors with regard to the prediction of PCa (Tables 2 and 3). However, when the malignancy risk was assessed based on nodule TICs only, there was no evidence to show that any of these factors is significantly better than the others. Moreover, certain other indices that were found to be significant in previous studies on PCa⁹ and liver^{15,16} and breast¹⁷ cancer did not appear significant in our findings,

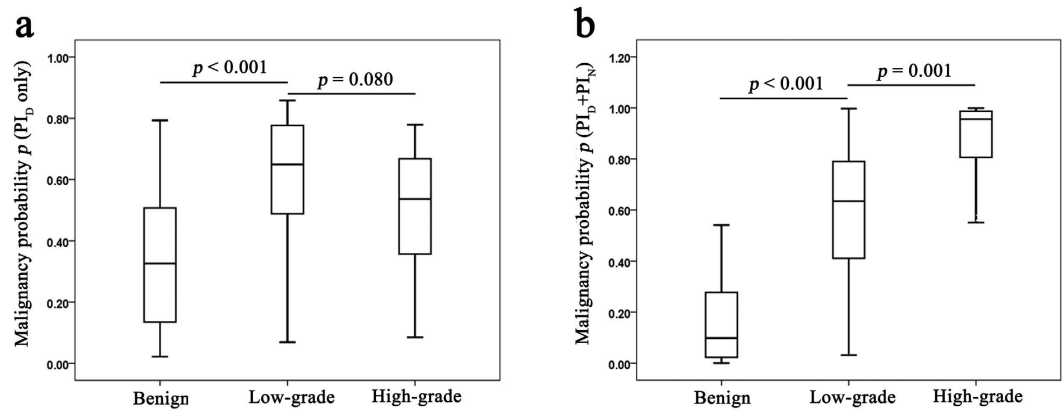


Figure 4. Box plot analysis of the probability of malignancy (p) based on (a) nodule peak intensity (PI) only and (b) normal peripheral zone (PZ) PI in the benign ($n = 76$), low-grade ($n = 23$) and high-grade tumour ($n = 31$) groups.

for example, AT (Tables 2 and 3). It is possible that if the inter-patient variation is eliminated or heterogeneity is adjusted for, the diagnostic accuracy of these factors for PCa may improve.

In CETRUS recordings, the entire prostate is represented by groups of data points; moreover, current studies often focus on the PZ hyperperfusion region rather than the whole prostate and do not conduct tissue analysis of other normal tissue^{18–20}. Here, we show that incorporating normal tissue TICs could significantly improve the diagnostic accuracy of nodule TICs for PCa detection (Fig. 2a,b). This is consistent with the finding that including background information enhances the discriminative ability of MRI for PCa¹¹. Interestingly, the other TIC parameters, such as MTT and TPH, improved the prediction of PCa by themselves, but incorporation of the corresponding normal PZ parameters did not improve PCa prediction (Table 3). This finding indicates that “background” prostate PZ perfusion characteristics affect the “Y-axis” intensity parameters of TICs, such as PI or AUC, but they do not affect the “X-axis” time parameters such as MTT and TPH. Our results also demonstrate that low nodule TIC values are suggestive of a potential malignancy in the presence of low normal PZ TIC values. Thus, it is not feasible to set any standard diagnostic threshold values for nodules or normal parameters (Fig. 3a,b).

The incorporation of PI_D plus PI_N or AUC_D plus AUC_N significantly affected the differentiation ability of TICs. However, it not clear whether the TIC values are useful for the precise assessment of cancer aggressiveness, which is commonly estimated by the Gleason score and largely influences PCa management^{21,22}. Moreover, the contrast-enhanced CETRUS findings for the PCa lesions showed various patterns according to tumour vascularity^{23,24} and aggressiveness^{25,26}; this is indicative of the heterogeneity of this cancer. In our study, incorporating TICs enabled the differentiation of low-grade tumours ($n = 23$) from high-grade ones ($n = 31$) (Fig. 4b). This finding indicates that normal PZ TICs play a novel role in the assessment of cancer aggressiveness.

This study had several limitations. Firstly, the use of TICs to assess transition zone tumours has not been investigated. Given that the majority of PCa’s arise in the PZ, this is a major limitation of this study. Secondly, ultrasound-guided prostate biopsy has inevitable false positive and false negative outcomes, which may have affected the final results of our study. Thirdly, the validity of the cancer aggressiveness assessment should be further tested in a large, prospective and multi-cohort study.

In conclusion, our findings demonstrate that incorporating the perfusion characteristics of normal PZ tissue may enable the identification of malignancies based on the quantitative TIC parameters of CETRUS. Thus, this is a novel approach that uses inter-patient differences for PCa prediction and assessment of cancer aggressiveness.

References

- Jemal, A. *et al.* Global cancer statistics. *CA Cancer J Clin* **61**, 69–90 (2011).
- Blute, M. L. *et al.* Use of Gleason score, prostate specific antigen, seminal vesicle and margin status to predict biochemical failure after radical prostatectomy. *J Urol* **165**, 119–125 (2001).
- Linden, R. A. *et al.* Contrast enhanced ultrasound flash replenishment method for directed prostate biopsies. *J Urol* **178**, 2354–2358 (2007).
- Bjurlin, M. A. *et al.* Optimization of initial prostate biopsy in clinical practice: sampling, labeling and specimen processing. *J Urol* **189**, 2039–2046 (2013).
- Zhao, H. X. *et al.* The value and limitations of contrast-enhanced transrectal ultrasonography for the detection of prostate cancer. *Eur J Radiol* **82**, e641–647 (2013).
- Sano, F. & Uemura, H. The utility and limitations of contrast-enhanced ultrasound for the diagnosis and treatment of prostate cancer. *Sensors (Basel)* **15**, 4947–4957 (2015).
- Russo, G. *et al.* Angiogenesis in prostate cancer: onset, progression and imaging. *BJU Int* **110**, E794–808 (2012).
- McClure, P. *et al.* In-vitro and in-vivo diagnostic techniques for prostate cancer: a review. *J Biomed Nanotechnol* **10**, 2747–2777 (2014).
- Zhu, Y. *et al.* Contrast-enhanced harmonic ultrasonography for the assessment of prostate cancer aggressiveness: a preliminary study. *Korean J Radiol* **11**, 75–83 (2010).
- Jung, E. M. *et al.* First results of endocavity evaluation of the microvascularization of malignant prostate tumors using contrast enhanced ultrasound (CEUS) including perfusion analysis: first results. *Clin Hemorheol Microcirc* **52**, 167–177 (2012).

11. Litjens, G. J. *et al.* Interpatient variation in normal peripheral zone apparent diffusion coefficient: effect on the prediction of prostate cancer aggressiveness. *Radiology* **265**, 260–266 (2012).
12. DeLong, E. R., DeLong, D. M. & Clarke-Pearson, D. L. Comparing the areas under two or more correlated receiver operating characteristic curves: a nonparametric approach. *Biometrics* **44**, 837–845 (1988).
13. Hanley, J. A. & McNeil, B. J. A method of comparing the areas under receiver operating characteristic curves derived from the same cases. *Radiology* **148**, 839–843 (1983).
14. Klotz, L. & Emberton, M. Management of low risk prostate cancer-active surveillance and focal therapy. *Nat Rev Clin Oncol* **11**, 324–334 (2014).
15. Furuichi, Y. *et al.* Obliteration of gastric varices improves the arrival time of ultrasound contrast agents in hepatic artery and vein. *J Gastroenterol Hepatol* **28**, 1526–1531 (2013).
16. Kim, M. Y. *et al.* Hepatic vein arrival time as assessed by contrast-enhanced ultrasonography is useful for the assessment of portal hypertension in compensated cirrhosis. *Hepatology* **56**, 1053–1062 (2012).
17. Poma, S. & Longo, A. The clinician's role in the diagnosis of breast disease. *J Ultrasound* **14**, 47–54 (2011).
18. Postema, A. *et al.* Ultrasound modalities and quantification: developments of multiparametric ultrasonography, a new modality to detect, localize and target prostatic tumors. *Curr Opin Urol* **25**, 191–197 (2015).
19. Ahmed, H. U. *et al.* Can we deliver randomized trials of focal therapy in prostate cancer? *Nat Rev Clin Oncol* **11**, 482–491 (2014).
20. Muller, B. G., van den Bos, W., Pinto, P. A. & de la Rosette, J. J. Imaging modalities in focal therapy: patient selection, treatment guidance, and follow-up. *Curr Opin Urol* **24**, 218–224 (2014).
21. Narain, V. *et al.* How accurately does prostate biopsy Gleason score predict pathologic findings and disease free survival? *Prostate* **49**, 185–190 (2001).
22. Freedland, S. J. *et al.* Adjuvant and salvage radiotherapy after prostatectomy: American Society of Clinical Oncology clinical practice guideline endorsement. *J Clin Oncol* **32**, 3892–3898 (2014).
23. Sano, F. *et al.* Contrast-enhanced ultrasonography of the prostate: various imaging findings that indicate prostate cancer. *BJU Int* **107**, 1404–1410 (2011).
24. Uemura, H. *et al.* Usefulness of perflubutane microbubble-enhanced ultrasound in imaging and detection of prostate cancer: phase II multicenter clinical trial. *World J Urol* **31**, 1123–1128 (2013).
25. Mitterberger, M. *et al.* Comparison of contrast enhanced color Doppler targeted biopsy to conventional systematic biopsy: Impact on Gleason score. *J Urol* **178**, 464–468 (2007).
26. Jiang, J., Chen, Y. Q., Zhu, Y. K., Yao, X. H. & Qi, J. Factors influencing the degree of enhancement of prostate cancer on contrast-enhanced transrectal ultrasonography: correlation with biopsy and radical prostatectomy specimens. *Br J Radiol* **85**, e979–e986 (2012).

Acknowledgements

This work was supported by the Research Project of Jiangsu Province of TCM (YB2015020), the Jiangsu Provincial Six Talent Peaks Project (2014-WSN-016), and the Research Project of Jiangsu Province Hospital of TCM (Y14033).

Author Contributions

H.H. and L.-P.Y. conceived and designed the study; H.H., Z.-G.Z., M.Z. and Y.Z. acquired the data; L.-S.C. and H.-B.L. controlled the quality of data; Z.-Q.Z. and H.H. analysed and interpreted the data; H.H., Z.-Q.Z., M.Z. and Y.Z. performed the statistical analyses; H.H. and Z.-Q.Z. wrote the paper; all the authors contributed to this paper. H.H. and Z.-Q.Z. contributed equally to this work.

Additional Information

Competing financial interests: The authors declare no competing financial interests.

How to cite this article: Huang, H. *et al.* Contrast-enhanced transrectal ultrasound for prediction of prostate cancer aggressiveness: The role of normal peripheral zone time-intensity curves. *Sci. Rep.* **6**, 38643; doi: 10.1038/srep38643 (2016).

Publisher's note: Springer Nature remains neutral with regard to jurisdictional claims in published maps and institutional affiliations.



This work is licensed under a Creative Commons Attribution 4.0 International License. The images or other third party material in this article are included in the article's Creative Commons license, unless indicated otherwise in the credit line; if the material is not included under the Creative Commons license, users will need to obtain permission from the license holder to reproduce the material. To view a copy of this license, visit <http://creativecommons.org/licenses/by/4.0/>

© The Author(s) 2016